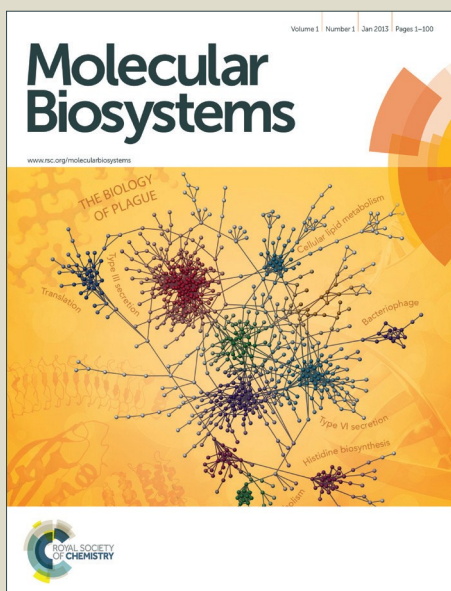


# Molecular BioSystems

Accepted Manuscript



This is an *Accepted Manuscript*, which has been through the Royal Society of Chemistry peer review process and has been accepted for publication.

*Accepted Manuscripts* are published online shortly after acceptance, before technical editing, formatting and proof reading. Using this free service, authors can make their results available to the community, in citable form, before we publish the edited article. We will replace this *Accepted Manuscript* with the edited and formatted *Advance Article* as soon as it is available.

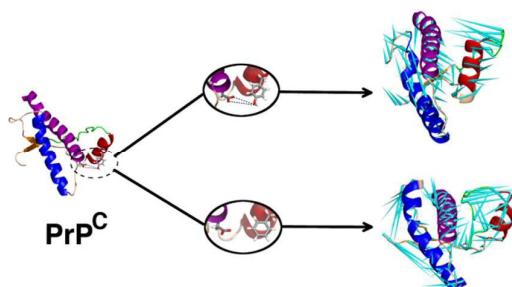
You can find more information about *Accepted Manuscripts* in the [Information for Authors](#).

Please note that technical editing may introduce minor changes to the text and/or graphics, which may alter content. The journal's standard [Terms & Conditions](#) and the [Ethical guidelines](#) still apply. In no event shall the Royal Society of Chemistry be held responsible for any errors or omissions in this *Accepted Manuscript* or any consequences arising from the use of any information it contains.



[www.rsc.org/molecularbiosystems](http://www.rsc.org/molecularbiosystems)

## Table of Content (TOC) Image



Loss of a key hydrogen bond between H1 and H3 causes marked changes in structure and dynamical behavior of PrP<sup>C</sup>.

**Perturbations in inter-domain associations may trigger onset of  
pathogenic transformations in PrP<sup>C</sup>: insights from atomistic  
simulations**

Sneha Menon and Neelanjana Sengupta \*

*Physical Chemistry Division, CSIR-National Chemical Laboratory, Pune 411008, India*

---

\* Correspondence: [n.sengupta@ncl.res.in](mailto:n.sengupta@ncl.res.in)

**Abstract**

Conversion of the predominantly  $\alpha$ -helical cellular prion protein ( $\text{PrP}^{\text{C}}$ ) to the misfolded  $\beta$ -sheet enriched Scrapie form ( $\text{PrP}^{\text{Sc}}$ ) is a critical event in prion disease pathogenesis. However, the conformational triggers that lead to the isoform conversion ( $\text{PrP}^{\text{C}}$  to  $\text{PrP}^{\text{Sc}}$ ) remain obscure, and conjectures about the role of unusually hydrophilic, short helix H1 of the C-terminal globular domain in the transition are varied. Helix H1 is anchored to helix H3 *via* a few stabilizing polar interactions. We have employed fully atomistic molecular dynamics simulations to study the effects triggered by a minor perturbation in the network of these non-bonded interactions in  $\text{PrP}^{\text{C}}$ . The elimination of just one of the key H1-H3 hydrogen bonds led to a cascade of conformational changes that are consistent with those observed in partially unfolded intermediates of  $\text{PrP}^{\text{C}}$ , with pathogenic mutations and at low pH environments. Our analyses reveal that the perturbation results in enhanced conformational flexibility of the protein. The resultant enhancement in the dynamics leads to overall increased solvent exposure of the hydrophobic core residues and concomitant disruption of H1-H3 inter-domain salt bridge network. This study lends credence to the hypothesis that perturbing the cooperativity of the stabilizing interactions in the  $\text{PrP}^{\text{C}}$  globular domain can critically affect its dynamics and may lead to structural transitions of pathological relevance.

**Keywords:**  $\text{PrP}^{\text{C}}$ , conformational transition, helix H1, hydrogen bond, inter-helix salt bridge, molecular dynamics simulation

Prions are proteinaceous infectious agents that cause fatal neurodegenerative diseases. These diseases, collectively termed as transmissible spongiform encephalopathies (or TSEs), include Creutzfeldt–Jakob disease, fatal familial insomnia, Gerstmann–Sträussler–Scheinker disease, Kuru in humans, scrapie in sheep, and bovine spongiform encephalopathy in cattle.<sup>1</sup> Such diseases occur as sporadic, acquired or inherited disorders hallmarked by the accumulation of an abnormal isoform of the prion protein.<sup>1, 3, 4</sup> According to the “protein-only” hypothesis, prion diseases arise from conformational changes in the normal isoform of cellular prion protein (PrP<sup>C</sup>) to a protease-resistant, pathogenic form called Scrapie (PrP<sup>Sc</sup>).<sup>3, 5</sup> The PrP<sup>Sc</sup> template has the ability to further recruit cellular isoforms of PrP<sup>C</sup> and subsequently induce them to alter their conformation to the misfolded form, thus ensuring self-propagation.<sup>1, 3, 6</sup>

The cellular prion protein, PrP<sup>C</sup>, is a highly conserved cell surface glycoprotein of ~210 amino acids that is bound to the cell membrane by a glycosylphosphatidylinositol (GPI) anchor at its C-terminal residue.<sup>7</sup> The N-terminal domain of PrP<sup>C</sup> is largely disordered, while the C-terminal region consists of a structured, globular domain. The globular domain, depicted in Figure 1b, is composed of two short  $\beta$ -strands, S1 (Y<sub>128</sub>MLG<sub>131</sub>) and S2 (V<sub>161</sub>YYR<sub>164</sub>), forming an anti-parallel  $\beta$ -sheet, and three  $\alpha$ -helices, H1 (D<sub>144</sub>YEDRYRENM<sub>154</sub>), H2 (N<sub>173</sub>NFVHDCVNITIKQHTVTTTTTK<sub>194</sub>) and H3 (E<sub>200</sub>TDVKMMERVVEQMCITQYERESQAYYQR<sub>228</sub>), with H2 and H3 covalently bridged by a disulfide-bond between Cys179 and Cys214.<sup>8</sup> The structure of the scrapie form, PrP<sup>Sc</sup>, is poorly defined as its insolubility and high conformational heterogeneity eludes high-resolution structural analysis techniques.<sup>9</sup> However, it is known that PrP<sup>Sc</sup> has substantial  $\beta$ -sheet content and reduced  $\alpha$ -helical content compared to the native form, which implies that the structural transition of PrP<sup>C</sup> to PrP<sup>Sc</sup> involves large conformational rearrangements.<sup>10</sup>

The conformational changes that drive PrP<sup>C</sup> to its pathogenic PrP<sup>Sc</sup> counterpart, as well as the mechanistic details of PrP<sup>Sc</sup> self-propagation have not yet been established.<sup>9</sup> Several models have been proposed for the structure of PrP<sup>Sc</sup> that provide clues on the fibrillation and oligomerization processes.<sup>11-14</sup> However, a point of contention concerns the regions in PrP<sup>C</sup> that harbor residue sequences vulnerable to conformational changes thereby facilitating initial seeding and further promoting fibrillar growth. Previous studies have suggested that the S1H1S2 region in PrP<sup>C</sup> plays a crucial role in the structural transition.<sup>11, 12, 15-17</sup> Interestingly, based on experimental and computational studies, views have also emerged about the potential role of H2 and H3 in the conversion of PrP<sup>C</sup> to PrP<sup>Sc</sup>.<sup>18-23</sup> The PrP<sup>C</sup> structure is stabilized by a core of hydrophobic residues, together with many salt-bridge and hydrogen-bonding interactions between the secondary structure elements.<sup>8, 24-26</sup> A number of pathogenic mutations reside in the hydrophobic core of PrP<sup>C</sup> that display varied effects on the mature protein.<sup>27</sup> Numerous studies indicate that perturbations to the structure, brought about by amino acid point mutations and changes in environmental conditions such as pH, temperature and presence of denaturants can substantially destabilize the PrP<sup>C</sup> conformer, affect its thermodynamic stability and induce structural transformations of pathological significance.<sup>28-31</sup>

In the globular domain of PrP<sup>C</sup>, helix H1 has certain intriguing properties<sup>32</sup> and its plausible roles in triggering the onset of TSEs has been the central topic in a series of experimental and computational studies.<sup>33-41</sup> In contrast with other helices usually found in globular proteins, H1 is characterized by a large abundance of hydrophilic, solvent exposed residues, making it the most soluble of all the protein  $\alpha$ -helices found in the PDB.<sup>32</sup> Circular dichroism (CD) and Nuclear magnetic resonance (NMR) studies of the isolated forms of H1 report its extreme stability, and thereby suggest the lack of its role in PrP<sup>Sc</sup> generation.<sup>34</sup>

Conversely, molecular modeling studies have proposed a model of PrP<sup>Sc</sup> aggregate, namely the  $\beta$ -nucleation model in which helix H1 unravels and favorably adopt  $\beta$ -sheet conformations.<sup>32</sup> These aggregates whose core consists of hydrophilic H1 components are mainly stabilized by the formation of inter-molecular salt-bridges between H1 residues. Many experimental and computational studies have postulated that a key molecular event in PrP<sup>C</sup> misfolding is the detachment of the S1H1S2 region from the H2H3 subdomain.<sup>17, 42-45</sup> Further, evidence from computer simulations suggests that a partially unfolded intermediate of the globular prion domain that is a possible candidate for PrP aggregation, displays the detachment and high mobility of the H1 from the relatively stable core formed by helices H2 and H3.<sup>17</sup> Such an analogous behavior has also been observed in simulation studies of PrP<sup>C</sup> in response to low pH as well as in some disease-associated mutants.<sup>15, 16, 46-48</sup> These studies suggest that interactions between the helices H1 and H3 could be playing significant roles in the conformational propensities of PrP<sup>C</sup>.

We point out that all mammalian species of the prion protein are highly conserved in sequence and architecture.<sup>8</sup> This is evident from a superimposition of PDB structures corresponding to different species<sup>8, 49-51</sup> as shown in Figure 1a, as well as the RMSD and percent identity values reported in Table S1 in the Electronic Supplementary Information (ESI). Local differences in the backbone conformations are manifested in the C-terminal of helix H3, the loop between S2 and H2 and the orientation of H1. Helix H1, owing to its charged nature, does not contribute to the hydrophobic core and is engaged in a cluster of electrostatic interactions, stabilizing the tertiary structure. Three non-local salt bridges E146-K204, E146-R208 and R156-D202 connect the stable H2H3 core with the more flexible domain consisting of H1 and strands S1 and S2. The interface of H1 (C-terminal) and H3 consists of three polar residues Y149, Y150 and N153. Of these residues, residue Y149 is

involved in an inter-helix side chain (H1H3) hydrogen-bonding interaction with residue D202. Residue Y150 forms a hydrogen bond with P137 that is located in the S1H1 loop region, while residue N153 forms an intra-helical backbone hydrogen bond with Y149. These interactions involving H1 residues are depicted in Figure S1. We have also reported the inter-residue distances corresponding to the aforementioned interactions in different prion proteins in Table S2, and additionally a pictorial representation of some key interactions in the superimposed structures in Figure S2. We note here that although the hydrogen bond Y149-D202 is not reported in the NMR structure of human prion protein used in this work, it is highly likely to form the bond during the course of an unbiased MD simulation.

Molecular dynamics (MD) simulations have been extensively used to provide an atomistic understanding of the structural, dynamical and self-assembly propensities of amyloidogenic proteins.<sup>13, 52-57</sup> In this study, using fully atomistic molecular dynamics (MD) simulations, we have studied the conformational and dynamical implications of a minor perturbation of H1 interactions, namely the loss of a single side chain-side chain hydrogen bond Y149-D202, that links H1 with the rest of the globular domain of PrP<sup>C</sup>. This perturbation was brought about by the replacement of residue Y149 with phenylalanine. Phenylalanine is identical to tyrosine except for the absence of the –OH group, which thus effectively obliterates the possibility of forming the Y149-D202 hydrogen bond in the artificially mutated system Y149F. Moreover, this replacement largely bypasses volume constraints without drastically affecting the structure of the protein. Such a minor perturbation could also be induced by stochastic, thermal or dynamical fluctuations or alterations to the solvent conditions. With 0.5  $\mu$ s of simulated data in each case and the dominant clusters elicited from Principal Component Analysis (PCA), we have evaluated and compared the conformational and dynamical behavior of the globular C-terminal domain of

PrP<sup>C</sup> in its native form (Figure 1b) with that of the singly mutated form with the Y149F mutation in H1 (Figure 1c). Our analyses show that this apparently small perturbation in H1-H3 interaction can result in conformational changes causing an overall weakening of the structural stability of PrP<sup>C</sup>. The hydration of the hydrophobic core and weakening of H1-H3 salt-bridge propensities due to the perturbation suggests a cooperative interplay in the network of these associations in maintaining structural stability of the protein. Interestingly, the decay of the internal associations resulted in marginal decrease in the degree of helicity, and a small overall increase in the length of the  $\beta$ -sheet domains. These changes in structure and dynamics are in agreement with the conformational changes observed at low pH, high temperature environments and in response to pathogenic point mutations.<sup>15, 16, 30, 31, 46-48</sup> Our results suggest that the origins of PrP<sup>C</sup> to PrP<sup>Sc</sup> transition may be present in stochastic perturbations to the native network of interactions that stabilize the PrP form.

## Methods

### System setup and MD Simulations

The NMR structure of the C-terminal domain (residues 125-228) of human PrP<sup>C</sup> (PDB entry – 1QM2) determined by Zahn et al.<sup>8</sup> were chosen as the initial structure for wild type prion protein (hereafter WT). A variant of the protein was obtained by replacing the Tyr residue at position 149 of the WT protein with a residue of Phe, to yield the Y149F system. The NH<sup>3+</sup> and COO<sup>-</sup> groups were added to the N and C-termini of the protein and three Na<sup>+</sup> counterions were used to neutralize the systems. Each system was solvated explicitly in a cubic box containing approximately 9600 TIP3P water molecules<sup>58</sup> and simulated under periodic boundary conditions. The systems were simulated using the NAMD2.8 simulation package<sup>59</sup> with the CHARMM22 all-atom force field with CMAP correction<sup>60</sup>. A time step of 2 fs was

used. A constant temperature of 310 K was maintained using Langevin dynamics with a collision frequency of  $1\text{ps}^{-1}$ . A pressure of 1 atmosphere was maintained using the Nosé-Hoover algorithm.<sup>61</sup> Covalent bonds involving hydrogen atoms were constrained using the SHAKE algorithm.<sup>62</sup> Long-range electrostatic interactions were computed by particle-mesh Ewald (PME) method.<sup>63</sup> The cutoff for non-bonded interactions was 12 Å, with smooth truncation starting from 10 Å. The systems were initially energy minimized for 15 000 steps on the basis of the conjugate gradient method followed by simulations in the isothermal-isobaric ensemble for 100 ns each. Five independent MD simulations were performed for WT and Y149F to generate trajectories of 100 ns each, amounting to a total of 0.5 μs of simulation time for each system. One control simulation trajectory was generated for each of the systems with the same simulation protocols described above, using the AMBER force field.<sup>64</sup>

### Principal Component Analysis

Principal component analysis (PCA) of the combined trajectories of WT and Y149F was performed to capture the motional complexity of the systems using the Carma program.<sup>65</sup> PCA is a widely used technique to obtain functionally relevant collective motions from MD simulation ensembles.<sup>66-70</sup> The analysis is based on the diagonalization of the variance-covariance matrix of atomic fluctuations along simulation trajectory. The eigenvectors and eigenvalues obtained from the diagonalization represent the various modes of motions and can be used to cluster the ensemble of structures. The eigenvectors corresponding to the largest eigenvalues are the ‘Principal Components’ (PC) that describe the largest amplitude collective motions of the protein. The probability distributions of the first two principal components (PC1 and PC2) corresponding to the  $C_{\alpha}$  atomic fluctuations are used to calculate

the free energy using the following equation,

$$\Delta G = -k_B T \ln \left[ \frac{p}{p_{\max}} \right] \quad (1)$$

where  $k_B$  is the Boltzmann's constant;  $T$  is the absolute temperature;  $p$  is the probability distribution of the first two principal components; and  $p_{\max}$  is the maximum probability.

The two extreme projections sampled along the trajectory on PC1 were further used to build porcupine plots that depict a graphical view of the dominant motion represented by the most populated cluster. In a porcupine plot, each  $C_\alpha$  atom has a cone pointing in the direction of its motion along the trajectory; the length of the cone represents the amplitude of the motion. The plots were generated using PyMOL.<sup>71</sup>

### Dynamic Cross Correlation Analysis

To identify the protein regions whose motions are correlated with one another, the cross-correlation of the atomic fluctuations obtained for the most populated cluster was obtained from PCA. The pairwise cross-correlation coefficient,  $C_{ij}$ , for the displacement of all  $C_\alpha$  atom pairs,  $i$  and  $j$ , is given by

$$C_{ij} = \frac{\langle \Delta r_i \cdot \Delta r_j \rangle}{\sqrt{\langle \Delta r_i^2 \rangle \langle \Delta r_j^2 \rangle}} \quad (2)$$

where  $\Delta r_i$  and  $\Delta r_j$  are the displacement vectors of the atoms  $i$  and  $j$ , from their mean positions respectively, which is determined from all configurations in the cluster. All frames of the cluster are superimposed on the initial structure and a matrix of all atom-wise cross-correlations is generated. The elements of the matrix are displayed in a graphical

representation termed as a ‘dynamic cross-correlation map’ (DCCM). The value of  $C_{ij} = 1$  for completely positively correlated motion while  $C_{ij} = -1$  for completely negatively correlated motion. Positively correlated residues move in the same direction, whereas negatively correlated residues move in the opposite direction. The magnitude of the cross-correlations of fluctuations of backbone  $C_{\alpha}$  atoms was calculated and plotted using the Bio3D Package.<sup>72</sup>

### Configurational entropy

We have calculated the configurational entropy per  $C_{\alpha}$  atom of the WT and Y149F systems using Schlitter’s method<sup>73</sup> as implemented in the Carma<sup>65</sup> program. According to Schlitter’s formula, the absolute entropy  $S$  is approximated as,

$$S_{abs} < S = \frac{1}{2} k_B \ln \det \left[ 1 + \frac{k_B T e^2}{\hbar^2} M \sigma \right] \quad (3)$$

Here,  $k_B$  is the Boltzmann’s constant;  $\hbar$  is Planck’s constant reduced by  $2\pi$ ;  $T$  is the absolute temperature;  $e$  is the Euler value;  $M$  is the diagonal mass matrix of rank  $3N$ ; and  $\sigma$  is the covariance matrix of the atomic positional fluctuations.

## Results and Discussion

### I. Conformational integrity

We have studied conformational and dynamical changes in the PrP<sup>C</sup> globular domain brought about by an elimination of an inter-domain hydrogen bond, namely Y149-D202, *via* a tyrosine to phenylalanine mutation at the residue position 149. In Figure 2a, we compare the

probability distributions of the side chain interaction energies of residue pairs Y149-D202 and F149-D202, belonging to the native and the mutated systems, respectively. Mean non-bonded interaction energies between these residues in the WT and Y149F systems are  $-11.46 (\pm 7.66)$  and  $-0.87 (\pm 0.94)$  kcal mol<sup>-1</sup>, respectively. Overall, the loss of the inter-domain H-bond between helices H1 and H3 causes a significant weakening of the side chain interactions. To compare the conformational stabilities, the root-mean-square-deviation (RMSD) of the backbone atoms was calculated for the two systems. In Figure 2b, we have plotted the RMSD of the backbone atoms of the WT and Y149F proteins relative to the initial structure over the simulation timescale, averaged over the five independent runs. The average RMSD of the mutant Y149F is markedly higher than that of WT system over the entire timescale, indicating that compared to the WT, marked conformational changes occur in the mutant system. The mean RMSD values for the WT and the Y149F systems, averaged over the last 80 ns, are  $3.22 (\pm 0.10)$  Å and  $3.97 (\pm 0.18)$  Å, respectively. We further compared the cumulative configurational entropy per C<sub>α</sub> atom as a measure of the extent of disorder of the two systems. As depicted in Figure 2c, the net configurational entropy of Y149F is larger than that of WT. The mean configurational entropy per C<sub>α</sub> atom for the WT and the Y149F systems, averaged over the last 2 ns, is  $32.94 (\pm 0.12)$  and  $34.13 (\pm 0.13)$  JK<sup>-1</sup>mol<sup>-1</sup>, respectively. Thus, the loss of the single H1-H3 hydrogen bond induces fluctuations and conformational disorder in PrP<sup>C</sup>. In Figure S3, we have depicted the interaction energy between residues 149 and 202, the configurational entropy per C<sub>α</sub> atom averaged over the trajectories along the simulation time in the WT and the Y149F systems, along with the corresponding standard deviations.

We also evaluated the above characteristics for the control simulation generated with

the AMBER force field, which is presented in Figure S4. The probability distribution of the side chain interaction energies, depicted in Figure S4a, indicates that the interaction strength of residue pair F149-D202 of the mutant is significantly reduced as compared to the WT residue pair Y149-D202. The mean interaction strengths in the WT and the Y149F systems are  $-13.765 (\pm 6.96)$  and  $-0.92 (\pm 0.84)$  kcal mol<sup>-1</sup>, respectively, and therefore comparable to the values obtained with CHARMM. We note here that the RMSD trends obtained for AMBER trajectories show a higher deviation for the WT. However, similar to the corresponding data obtained with CHARMM, the configurational entropy per C<sub>α</sub> atom of the mutant is higher than that of the WT system. The mean configurational entropy averaged over the last 2 ns of the WT and Y149F systems simulated with AMBER are  $36.55 (\pm 0.09)$  and  $38.84 (\pm 0.12)$  JK<sup>-1</sup>mol<sup>-1</sup> respectively.

## II. Principal Component Analysis (PCA) and essential dynamics

PCA, as described in *Methods*, was performed on the simulation ensembles of the WT and Y149F systems. The overall flexibility of the two systems was calculated by the trace of the diagonalized covariance matrix of the C<sub>α</sub> atomic fluctuations. The trace values for the WT and Y149F systems were found to be 701.82 and 1042.92 Å<sup>2</sup>, respectively, suggesting that there is higher flexibility in the collective motion of the protein in Y149F as compared to that of WT. In Figure 3a and b, we present the free energy landscape projected on the first (PC1) and second (PC2) principal components, and provide snapshots of representative conformations of the most populated cluster of the two systems. In all further analyses, we considered the most populated clusters obtained from the PCA of the simulated systems for comparing the structural and dynamical characteristics of PrP<sup>C</sup> of the WT system and the

system with induced perturbations in inter-domain interactions.

To identify key differences in the modes of motion in the WT and Y149F systems, we generated porcupine plots from the extreme projections on PC1 generated from the simulation ensembles; these are presented in Figures 4a and b. The unidirectional motion of the helices H1 and H3 indicates dynamical correlation between them in the WT system. However, this correlation is largely lost in the perturbed Y149F system, and the two helices are observed to move in opposite directions. The S1H1 loop, preceding helix H1, exhibits large amplitude displacements in both the systems, albeit in opposite directions. In WT, the S1H1 loop moves in a direction towards the H2H3 sub domain with which it forms the hydrophobic core in PrP<sup>C</sup>. In Y149F, on the other hand, it moves in a direction away from H2H3 subdomain. Moreover, the short, anti-parallel  $\beta$ -sheet linked by a hydrogen bond network shows concerted motion. We note here that earlier studies have reported the movement of H1 and the S1H1 loop away from H3.<sup>15, 16, 47, 48</sup> However, we observed that S1H1 loop movement is opposite to that of H1. The helices H2 and H3 that together form bulk of the hydrophobic core do not move unidirectionally, but the magnitude of this displacement is low in both the systems. We remark here that H2 and H3 is connected by a disulfide bridge between residues Cys179 and Cys214. In Figure 5, we have plotted the distribution of the distance between the sulfur atoms of these residues. The mean distance between the two atoms increases from 4.99 ( $\pm 0.36$ ) Å in the WT, to 7.40 ( $\pm 0.68$ ) Å in the Y149F system. While the possibility of bond breakage cannot be assessed with classical simulations, this analysis indicates that the structural changes in the Y149F system markedly affects the stability attributed to the disulfide bridge.

To further corroborate the observed dynamics, we quantified the interatomic cross correlations of the fluctuations in C $_{\alpha}$  atomic positions of the two systems. In Figure 4c and d,

we have illustrated the Dynamic Cross-Correlation Map (DCCM) representing the correlated motions of WT and Y149F ensembles projected along PC1. In the WT, H1 is positively correlated with N-terminal of H3, in agreement with their concerted motion as a unit observed in the porcupine plot. On the other hand, in Y149F, H1 has a strong negative correlation with H3; interestingly, this correlation is of a higher degree with the N-terminal end of H3, which is the region of contact of H1 and H3. Further, helices H2 and H3 are anticorrelated with each other in WT and have less pronounced negative correlation in the mutant. The short, anti-parallel  $\beta$ -strands are positively correlated with each other in both the systems as they are connected by a hydrogen bond network and move in phase. These analyses show that small perturbation in the network of interactions in the PrP<sup>C</sup> domain can critically affect its flexibility and modes of internal motions.

### III. Hydration of the hydrophobic core

In PrP<sup>C</sup>, a tightly packed hydrophobic core consists of the twenty residues Met134, Pro137, Ile139, Phe141, Pro158, Val161, Phe175, Val176, Cys179, Val180, Ile184, Phe198, Val203, Met205, Met206, Val209, Met210, Cys213, Cys214 and Ile215.<sup>24</sup> These residues provide hydrophobic contacts between helices H2 and H3; between the S1H1 loop and H3; and between the anti-parallel  $\beta$ -sheet and H2 or H3. The hydrophobic core residues between helices H2-H3 and at the S1H1 loop-H3 interface are depicted in Figures 6a and b respectively. We note here that several pathogenic mutations are located in the hydrophobic core, and importantly, a number of studies relate the instability of the hydrophobic core to the early steps in the misfolding process.<sup>16, 27, 48</sup> Herein, we investigated how the dynamical changes induced by the minor perturbation in the H1-H3 interactions could affect the stability of the hydrophobic core. We first assessed the solvent-accessible surface area of the

hydrophobic core,  $SASA_{HC}$ , calculated within the VMD package<sup>74</sup> by running a spherical probe of 1.8 Å radius over the protein surface, as a measure of its compactness and solvent exposure. In Figure 6c, we depict the probability distributions of  $SASA_{HC}$  computed for the WT and Y149F. In Y149F, there is a clear shift of the  $SASA_{HC}$  of the hydrophobic core towards higher values; the peak positions in the WT and Y149F systems are centered at ~425 and ~550 Å<sup>2</sup>, respectively. We have plotted, in Figure S3c, the  $SASA$  of the hydrophobic core residues, averaged over the independent trajectories in each system as a function of simulation time, along with corresponding standard deviations. Thus, the perturbation caused by loss of a single H1-H3 hydrogen bond in Y149F effectively leads to about 30% increase in the solvent exposure of the hydrophobic core. We also analyzed the  $SASA_{HC}$  of the AMBER simulation trajectories the probability distributions of which are depicted in Figure S5. There is enhanced hydration of the Y149F system as compared to the WT, with the peak positions at ~325 and ~510 Å<sup>2</sup>, respectively, which is comparable to the observation with CHARMM. We note here that the  $SASA_{HC}$  increase is observed in Y149F despite the slightly higher hydrophobicity of phenylalanine compared to tyrosine. The increase, therefore, should be attributable to the increased conformational flexibility and the loss of structural coherence in the perturbed system.

To elucidate the residue-level changes, we present in Figure 6d, the residue-wise mean solvent accessible surface area, or  $SASA_{res}$ , of the individual hydrophobic core residues analyzed for the WT and Y149F systems. The comparison reveals that the mean  $SASA_{res}$  of residues Ile139, Pro158, Phe175, Val176, Cys179, Val180, Met205, Met206, Val209, Val210, Met213, Cys214 and Ile215 is higher in Y149F. Of these residues, Met205, Val209 and Met213 in H3 have hydrophobic interactions with residues of the S1H1 loop. This is commensurate with the observed decorrelated motion of H1 and H3 in Y149F that causes the

exposure of the H3 residues linked by hydrophobic contacts with the S1H1 loop. Residues Phe175, Val176, Val180 and Ile184 of H2 have hydrophobic interactions with residues Val203, Met206, Val210 and Ile215 of H3. The increased  $SASA_{res}$  of these residues shows that the stability of hydrophobic interactions in the H2H3 subdomain are affected due to increased solvent exposure. Helices H2 and H3 are connected by a disulfide bond formed between residues Cys179-Cys214 that also show an enhanced  $SASA_{res}$ . This suggests that the packing of helices H2 and H3 in the hydrophobic core is perturbed significantly in the Y149F system. Residue P158, located in the loop between H1 and S2, shows remarkable increase in  $SASA_{res}$  in Y149F as compared to the WT system. In the WT system, the side chain of P158 is oriented towards H3, which is part of the hydrophobic core, and thus shielded from the surrounding water. However, in Y149F, the enhanced dynamics and flexibility of the S1H1S2 region in a direction away from the hydrophobic core, results in exposure of the P158 side chain to solvent molecules. The analyses above shows that the dynamics of PrP<sup>C</sup> resulting from the perturbation of H1-H3 interaction and the resulting mobilities of the structural elements causes marked decrease in the stability of the hydrophobic core.

In addition, we analyzed two hydration sites previously identified by De Simone *et al.*<sup>75</sup> with tightly bound structurally conserved waters that are necessary in maintaining local elements of the PrP<sup>C</sup> fold. The water at site 1 mediates the interaction between the carbonyl of S132, the amide of V161 and the Q217 side chain oxygen; thus connecting three protein regions that belong to different secondary structure elements S1, S2 and H3, respectively. In Figure S6a, we have plotted the probability distributions of the distance between S132:O - V161:N in the dominant cluster of the two systems. The peak positions of the distribution are  $\sim 5.2$  Å and  $\sim 7$  Å for WT and Y149F systems, respectively. The increase in the distance between the backbones of S132 and V161 of  $\sim 2$ Å in Y149F indicates that the increased

fluctuations and dynamics in this system destabilize the water-mediated interaction at site 1. Another identified hydration site, with long residence time (exceeding 1ns) is located at the end of strand S2 and H2. This site bridges the backbone oxygen of residue F175 and the amide of R164; it also interacts with the side chain of D178. We analyzed the distance between the atoms of the F175:O - R164:N interaction; the probability distance distributions of this interaction are depicted in Figure S6b. Interestingly, the mutant exhibits a bimodal distribution with the higher peak position at  $\sim 5.5\text{\AA}$ , while the WT system has a peak position of  $\sim 7.5\text{\AA}$ . The reduced distance between the interacting atoms indicates that the water-mediated interaction at site 2 is strengthened in the mutant Y149F. We mention here that there is very little overlap of the hydrophobic core residues with the residues participating in these tightly bound hydration sites.

#### IV. Inter-domain salt bridge stability

The PrP<sup>C</sup> structure contains a diverse set of salt bridges that have been proposed to play an important role in stabilizing secondary structural elements and maintaining the overall tertiary fold.<sup>26</sup> Hence, disruption of the salt bridge network may substantially destabilize the folded conformation. To understand how a minor perturbation of the interactions that tether H1 to the rest of the protein may affect the stability of the salt bridge network, we examined the three non-local salt-bridges that anchor H1 to H3: E146-K204, E146-R208 and R156-D202. Previous studies have asserted that these salt-bridges contribute to the stabilization of PrP<sup>C</sup> and that their abolition, either due to protonation of the acidic amino acids in response to low pH or by relevant genetic mutations, decreases the stability of PrP<sup>C</sup> and favors misfolding.<sup>16, 26, 27, 76, 77</sup> In Figure 7a-c, we depict distributions of the salt bridge distances ( $d_{SB}$ ) between each pair in the WT and the perturbed Y149F system. In Y149F, the  $d_{SB}$

distributions shift to higher values compared to the unmutated system for all the three salt-bridge pairs. In Table 1, we have reported the mean values of the inter-residue distances and interaction energies of these salt-bridge forming residue pairs in the most populated cluster of the WT and Y149F systems. The interactions for all the three salt-bridges are weakened in Y149F as compared to the WT system.

We note here that the formation of stable salt-bridge networks is generally associated with a desolvation barrier.<sup>78-81</sup> Thus, the overall destabilization of the salt bridge network in Y149F may be commensurate with a higher local desolvation barrier resulting from the increased hydration accompanying the dynamical instability in this system. We probe this effect by comparing the protein-water radial distribution functions,  $g(r)$ , calculated between the oxygen atoms of solvent water molecules and the  $C_\beta$  atom of the salt-bridge forming residues for the WT and Y149F systems; these results are shown in Figures 7d-f. Commensurate with stronger salt-bridge interaction in the E146 – K204, E146 – R208 and R156 – D202 pairs in the WT, the first and second solvation peaks in  $g(r)$  are marginally weaker in this system compared to Y149F. These analyses illustrate how a minor loss in the H1-H3 association results in major perturbations within the salt-bridge network of the folded domain of PrP<sup>C</sup>.

## V. Secondary structural propensity

We finally attempt to understand if the disruption of H1-H3 interactions and the resulting conformational dynamics may cascade into secondary structural effects relevant for prion propagation. In Figure 8, we compare the residue-wise helical and  $\beta$ -sheet propensities of dominant clusters in the WT and Y149F systems, obtained with the STRIDE algorithm<sup>82</sup> in VMD<sup>74</sup>. The structure of helix H1 is found to be stable in both the WT and Y149F systems.

However, the region near the C-terminal end of H1, consisting of residues M<sub>154</sub>YR<sub>156</sub>, is labile. In the WT system, these residues formed a  $3_{10}$ -helix in about 20% of the conformations within the most populated cluster. On the other hand, in the Y149F system, these residues adopt  $\alpha$ -helical conformations. We note here that increased disorder is known to exist in residues D<sub>167</sub>EYSN<sub>171</sub> in the S2H2 loop.<sup>8</sup> Our analysis shows that these residues exhibit transient  $3_{10}$  helicity in both systems, but with a distinctly lower propensity in Y149F. We further note that experimental and computational studies have shown that residues at the C-terminal end of H2 are frustrated in their helical state.<sup>8</sup> However, surprisingly, we observe here that the N-terminal end of H2 up to the disulfide-bond forming residue, Cys179, undergoes structural loss in Y149F system, while the C-terminal region remains fairly stable. Furthermore, we observed that the lengths of the  $\beta$ -strands in Y149F were enhanced relative to the WT system. This was corroborated with an analysis of inter-strand backbone hydrogen bonds in S1 and S2; the donor-acceptor distance threshold for a hydrogen bond was 4.0 Å and the angle connecting the donor, hydrogen and the acceptor atoms was more than 135°. In the starting structure, the short anti-parallel  $\beta$ -sheet consists of four inter-strand backbone hydrogen bonds, namely, M129:N - Y163:O; M129:O - Y163:N and G131:N - V161:O and M134:N - N159:O. These hydrogen bonds are fairly stable in the WT system. In addition, two new hydrogen bonds, V161:N - G131:O and A133:N - N159:O, are observed in the Y149F system, resulting in a slight elongation of the native  $\beta$ -sheet. The glycine at the end of strand S1, which promotes a conserved  $\beta$ -bulge, was proposed to be a “negatively designed element”<sup>83</sup> to prevent edge-to-edge intermolecular  $\beta$ -sheet aggregation in PrP<sup>C</sup>.<sup>84</sup> Furthermore, residue R220 interacts with S132, thus sustaining the  $\beta$ -bulge in the edge strand S1. We remark here that the enhanced fluctuation of the S1H1 loop in Y149F causes the displacement of S132, which destabilizes the  $\beta$ -bulge. Interestingly, the disruption of the  $\beta$ -

bulge exposes the unsaturated amides and carbonyls on the edge strand S1, which results in the formation of the V161:N - G131:O bond. A fifth hydrogen bond, A133:N - N159:O is formed in Y149F. These additional hydrogen bonds in Y149F have the effect of elongating and stabilizing the native  $\beta$ -sheet. This observation is consistent with previous simulation studies on partially unfolded states of PrP<sup>C</sup>, effects of pathogenic mutations, and influence of low pH environment.<sup>17, 46</sup> The effect of perturbing inter-domain associations is thus manifested in notable secondary structural changes of the globular domain. However, it is appropriate to keep in mind that secondary structure propensities could be sensitive to force field effects. Therefore, the correlation between the conformational dynamics and secondary structural propensities yielded by MD trajectories generated with other atomistic force fields should also be compared.

## Conclusions

In this work, we have examined the effects of the disruption of a single hydrogen bond between the H1 and H3 helical domains on the overall behavior of the folded, C-terminal globular domain of PrP<sup>C</sup>. We observed that this relatively minor perturbation in the inter-domain association cascaded into several key conformational and dynamical effects. The effect is manifested in the dynamics of the various secondary structural domains, which in turn resulted in increased solvent exposure of residues of the hydrophobic core and overall reduced stability of the inter-domain salt bridges. The changes were further accompanied by an overall helical destabilization and subtle elongation of the  $\beta$ -strands, which could potentially mark the onset of conformational transitions to the PrP<sup>Sc</sup> forms. We note that the observed changes are consistent with the conformational changes observed in misfolding studies, at low pH or in studies with pathogenic mutations.<sup>15-17, 27, 48</sup>

As mentioned previously, earlier studies have highlighted the role of several inter-domain non-bonded interactions in the early structural determinants of PrP<sup>C</sup> to PrP<sup>Sc</sup> transition.<sup>17, 42-45, 77, 85</sup> Our study strongly underscores that the cooperative interplay of various non-bonded associations, particularly inter-helical hydrogen bonding between H1 and H3, hydrophobic contacts and salt bridge network, are necessary to maintain the structural integrity of the folded domain of PrP<sup>C</sup>. Small, transient perturbations in the network of these interactions may critically disrupt this cooperativity and thereby induce dynamical and conformational instabilities potentially leading to structures that are prone to pathogenic transitions. In the light of these findings, it could be useful to design anti-prion strategies that bias the folded state by reducing dynamical fluctuations and stabilizing key inter-domain associations. Further investigations on longer timescales, coupled with precise experimental measurements, are required to characterize the transient nature of the observed fluctuations, and the extent to which they are capable of modulating the heterogeneous pathways inherent to the PrP<sup>C</sup> to PrP<sup>Sc</sup> transition.

### **Acknowledgements**

Computational resources were obtained through funding from the CSIR 12<sup>th</sup> Five Year Plan ‘Multi-Scale Simulation and Modeling’ project (MSM; grant number CSC0129). S.M acknowledges her Ph.D. fellowship provided by the Department of Biotechnology through the Bioinformatics National Certification (BINC) examination. N.S acknowledges additional resources from the Center of Excellence in Polymers (CoEP-SPIRIT), established from funding received from the Department of Chemicals and Petrochemicals

## References

1. S. Liemann and R. Glockshuber, *Biochemical and Biophysical Research Communications*, 1998, 250, 187-193.
2. A. Aguzzi and A. M. Calella, *Physiological reviews*, 2009, 89, 1105-1152.
3. S. B. Prusiner, *Annual Review of Microbiology*, 1989, 43, 345-374.
4. S. B. Prusiner, *Science*, 1991, 252, 1515-1522.
5. C. Weissmann, *Journal of Biological Chemistry*, 1999, 274, 3-6.
6. S. B. Prusiner, *Proceedings of the National Academy of Sciences*, 1998, 95, 13363-13383.
7. N. Stahl, D. R. Borchelt, K. Hsiao and S. B. Prusiner, *Cell*, 1987, 51, 229-240.
8. R. Zahn, A. Liu, T. Lührs, R. Riek, C. von Schroetter, F. López García, M. Billeter, L. Calzolari, G. Wider and K. Wüthrich, *Proceedings of the National Academy of Sciences*, 2000, 97, 145-150.
9. R. Diaz-Espinoza and C. Soto, *Nat Struct Mol Biol*, 2012, 19, 370-377.
10. K. M. Pan, M. Baldwin, J. Nguyen, M. Gasset, A. Serban, D. Groth, I. Mehlhorn, Z. Huang, R. J. Fletterick and F. E. Cohen, *Proceedings of the National Academy of Sciences*, 1993, 90, 10962-10966.
11. H. Wille, M. D. Michelitsch, V. Guénebaut, S. Supattapone, A. Serban, F. E. Cohen, D. A. Agard and S. B. Prusiner, *Proceedings of the National Academy of Sciences*, 2002, 99, 3563-3568.
12. C. d. Govaerts, H. Wille, S. B. Prusiner and F. E. Cohen, *Proceedings of the National Academy of Sciences of the United States of America*, 2004, 101, 8342-8347.
13. M. L. DeMarco and V. Daggett, *Proceedings of the National Academy of Sciences of the United States of America*, 2004, 101, 2293-2298.

14. N. J. Cobb, F. D. Sönnichsen, H. McHaourab and W. K. Surewicz, *Proceedings of the National Academy of Sciences*, 2007, 104, 18946-18951.
15. M. L. DeMarco and V. Daggett, *Biochemistry*, 2007, 46, 3045-3054.
16. M. W. van der Kamp and V. Daggett, *Biophysical Journal*, 2010, 99, 2289-2298.
17. A. De Simone, A. Zagari and P. Derreumaux, *Biophysical Journal*, 2007, 93, 1284-1292.
18. R. I. Dima and D. Thirumalai, *Biophysical Journal*, 2002, 83, 1268-1280.
19. M. Adrover, K. Pauwels, S. Prigent, C. de Chiara, Z. Xu, C. Chapuis, A. Pastore and H. Rezaei, *Journal of Biological Chemistry*, 2010, 285, 21004-21012.
20. N. Chakroun, S. Prigent, C. A. Dreiss, S. Noinville, C. Chapuis, F. Fraternali and H. Rezaei, *The FASEB Journal*, 2010, 24, 3222-3231.
21. R. Tycko, R. Savtchenko, V. G. Ostapchenko, N. Makarava and I. V. Baskakov, *Biochemistry*, 2010, 49, 9488-9497.
22. J. Chen and D. Thirumalai, *Biochemistry*, 2013, 52, 310-319.
23. N. Chakroun, A. Fornili, S. h. Prigent, J. Kleinjung, C. i. A. Dreiss, H. Rezaei and F. Fraternali, *Journal of Chemical Theory and Computation*, 2013, 9, 2455-2465.
24. R. Riek, G. Wider, M. Billeter, S. Hornemann, R. Glockshuber and K. Wüthrich, *Proceedings of the National Academy of Sciences*, 1998, 95, 11667-11672.
25. J. Zuegg and J. E. Gready, *Biochemistry*, 1999, 38, 13862-13876.
26. W. C. Guest, N. R. Cashman and S. S. Plotkin, *Biochemistry and Cell Biology*, 2010, 88, 371-381.
27. M. W. van der Kamp and V. Daggett, *Journal of Molecular Biology*, 2010, 404, 732-748.
28. S. Liemann and R. Glockshuber, *Biochemistry*, 1999, 38, 3258-3267.

29. L. Calzolari and R. Zahn, *Journal of Biological Chemistry*, 2003, 278, 35592-35596.
30. E. El-Bastawissy, M. H. Knaggs and I. H. Gilbert, *Journal of Molecular Graphics and Modelling*, 2001, 20, 145-154.
31. S. Santini, J.-B. Claude, S. Audic and P. Derreumaux, *Proteins: Structure, Function, and Bioinformatics*, 2003, 51, 258-265.
32. M. P. Morrissey and E. I. Shakhnovich, *Proceedings of the National Academy of Sciences*, 1999, 96, 11293-11298.
33. J. O. Speare, T. S. Rush, M. E. Bloom and B. Caughey, *Journal of Biological Chemistry*, 2003, 278, 12522-12529.
34. J. Ziegler, H. Sticht, U. C. Marx, W. Müller, P. Rösch and S. Schwarzingler, *Journal of Biological Chemistry*, 2003, 278, 50175-50181.
35. G. J. Sharman, N. Kenward, H. E. Williams, M. Landon, R. J. Mayer and M. S. Searle, *Folding and Design*, 1998, 3, 313-320.
36. A. Liu, R. Riek, R. Zahn, S. Hornemann, R. Glockshuber and K. Wüthrich, *Peptide Science*, 1999, 51, 145-152.
37. E. M. Norstrom and J. A. Mastrianni, *Journal of Virology*, 2006, 80, 8521-8529.
38. S. Santini and P. Derreumaux, *Cellular and Molecular Life Sciences CMLS*, 2004, 61, 951-960.
39. J. Watzlawik, L. Skora, D. Frense, C. Griesinger, M. Zweckstetter, W. J. Schulz-Schaeffer and M. L. Kramer, *Journal of Biological Chemistry*, 2006, 281, 30242-30250.
40. H.-F. Ji, H.-Y. Zhang and L. Shen, *Journal of Biomolecular Structure and Dynamics*, 2005, 22, 563-570.
41. C. Camilloni, D. Schaal, K. Schweimer, S. Schwarzingler and A. De Simone,

- Biophysical Journal*, 2012, 102, 158-167.
42. S. Schwarzingler, A. H. C. Horn, J. Ziegler and H. Sticht, *Journal of Biomolecular Structure and Dynamics*, 2006, 23, 581-590.
43. F. Eghiaian, T. Daubenfeld, Y. Quenet, M. van Audenhaege, A.-P. Bouin, G. van der Rest, J. Grosclaude and H. Rezaei, *Proceedings of the National Academy of Sciences*, 2007, 104, 7414-7419.
44. J. H. Viles, D. Donne, G. Kroon, S. B. Prusiner, F. E. Cohen, H. J. Dyson and P. E. Wright, *Biochemistry*, 2001, 40, 2743-2753.
45. N. Kachel, W. Kremer, R. Zahn and H. R. Kalbitzer, *BMC structural biology*, 2006, 6, 16.
46. W. Chen, M. W. van der Kamp and V. Daggett, *Biochemistry*, 2010, 49, 9874-9881.
47. C. Cheng and V. Daggett, *Biomolecules*, 2014, 4, 181-201.
48. J. Guo, L. Ning, H. Ren, H. Liu and X. Yao, *Biochimica et Biophysica Acta (BBA) - General Subjects*, 2012, 1820, 116-123.
49. R. Riek, S. Hornemann, G. Wider, M. Billeter, R. Glockshuber and K. Wuthrich, *Nature*, 1996, 382, 180-182.
50. T. L. James, H. Liu, N. B. Ulyanov, S. Farr-Jones, H. Zhang, D. G. Donne, K. Kaneko, D. Groth, I. Mehlhorn, S. B. Prusiner and F. E. Cohen, *Proceedings of the National Academy of Sciences*, 1997, 94, 10086-10091.
51. F. López García, R. Zahn, R. Riek and K. Wüthrich, *Proceedings of the National Academy of Sciences*, 2000, 97, 8334-8339.
52. I. Autiero, M. Saviano and E. Langella, *Molecular BioSystems*, 2013, 9, 2118-2124.
53. S.-H. Chong, J. Yim and S. Ham, *Molecular BioSystems*, 2013, 9, 997-1003.
54. I. Autiero, E. Langella and M. Saviano, *Molecular BioSystems*, 2013, 9, 2835-2841.

55. N.-V. Buchete, R. Tycko and G. Hummer, *Journal of Molecular Biology*, 2005, 353, 804-821.
56. A. K. Jana, J. C. Jose and N. Sengupta, *Physical Chemistry Chemical Physics*, 2013, 15, 837-844.
57. A. K. Jana and N. Sengupta, *Biophysical Journal*, 2012, 102, 1889-1896.
58. W. L. Jorgensen, J. Chandrasekhar, J. D. Madura, R. W. Impey and M. L. Klein, *The Journal of Chemical Physics*, 1983, 79, 926-935.
59. L. Kale, R. Skeel, M. Bhandarkar, R. Brunner, A. Gursoy, N. Krawetz, J. Phillips, A. Shinozaki, K. Varadarajan and K. Schulten, *Journal of Computational Physics*, 1999, 151, 283-312.
60. A. D. Mackerell, *Journal of Computational Chemistry*, 2004, 25, 1584-1604.
61. S. E. Feller, Y. Zhang, R. W. Pastor and B. R. Brooks, *The Journal of Chemical Physics*, 1995, 103, 4613-4621.
62. J.-P. Ryckaert, G. Ciccotti and H. J. C. Berendsen, *Journal of Computational Physics*, 1977, 23, 327-341.
63. U. Essmann, L. Perera, M. L. Berkowitz, T. Darden, H. Lee and L. G. Pedersen, *The Journal of Chemical Physics*, 1995, 103, 8577.
64. D. Case, T. Darden, T. E. Cheatham III, C. Simmerling, J. Wang, R. Duke, R. Luo, R. Walker, W. Zhang and K. Merz, *University of California, San Francisco*, 142.
65. N. M. Glykos, *Journal of Computational Chemistry*, 2006, 27, 1765-1768.
66. Y.-S. Lin, G. Bowman, K. Beauchamp and V. Pande, *Biophysical Journal*, 2012, 102, 315-324.
67. S. Haider, G. N. Parkinson and S. Neidle, *Biophysical Journal*, 2008, 95, 296-311.
68. V. E. Fadouloglou, A. Stavrakoudis, V. Bouriotis, M. Kokkinidis and N. M. Glykos,

- Journal of Chemical Theory and Computation*, 2009, 5, 3299-3311.
69. L. Michel Espinoza-Fonseca, I. Ilizaliturri-Flores and J. Correa-Basurto, *Molecular BioSystems*, 2012, 8, 1798-1805.
70. S. Bhakat, A. J. M. Martin and M. E. S. Soliman, *Molecular BioSystems*, 2014, 10, 2215-2228.
71. W. L. Delano, 2002.
72. B. J. Grant, A. P. C. Rodrigues, K. M. ElSawy, J. A. McCammon and L. S. D. Caves, *Bioinformatics*, 2006, 22, 2695-2696.
73. J. Schlitter, *Chemical Physics Letters*, 1993, 215, 617-621.
74. W. Humphrey, A. Dalke and K. Schulten, *Journal of Molecular Graphics*, 1996, 14, 33-38.
75. A. De Simone, G. G. Dodson, C. S. Verma, A. Zagari and F. Fraternali, *Proceedings of the National Academy of Sciences of the United States of America*, 2005, 102, 7535-7540.
76. M. W. van der Kamp and V. Daggett, *Protein Engineering Design and Selection*, 2009, 22, 461-468.
77. K. Bamdad and H. Naderi-Manesh, *Biochemical and Biophysical Research Communications*, 2007, 364, 719-724.
78. R. Salari and L. T. Chong, *The journal of physical chemistry letters*, 2010, 1, 2844-2848.
79. H. Meuzelaar, M. Tros, A. Huerta-Viga, C. N. van Dijk, J. Vreede and S. Woutersen, *The journal of physical chemistry letters*, 2014, 5, 900-904.
80. R. Salari and L. T. Chong, *The Journal of Physical Chemistry B*, 2012, 116, 2561-2567.

81. J. C. Jose, P. Chatterjee and N. Sengupta, *PLoS ONE*, 2014, 9, e106883.
82. M. Heinig and D. Frishman, *Nucleic acids research*, 2004, 32, W500-W502.
83. J. S. Richardson and D. C. Richardson, *Proceedings of the National Academy of Sciences*, 2002, 99, 2754-2759.
84. A. De Simone, G. G. Dodson, F. Fraternali and A. Zagari, *FEBS Letters*, 2006, 580, 2488-2494.
85. L. Ning, J. Guo, N. Jin, H. Liu and X. Yao, *Journal of Molecular Modeling C7 - 2106*, 20, 1-8.

**Tables**

**Table 1.** Mean inter-residue distances,  $d$  (Å) and interaction energies,  $E$  (kcal mol<sup>-1</sup>) of the salt-bridge forming residues of the most populated cluster of the WT and Y149F systems. Standard deviations are provided within braces.

<i>Salt-bridge</i>	<i>d</i>		<i>E</i>	
	WT	Y149F	WT	Y149F
E146-K204	10.40 (±4.95)	13.47 (±2.58)	-21.21 (±32.38)	-1.45(±2.74)
E146-R208	8.30 (±4.26)	16.16 (±1.43)	-31.11 (±37.33)	-0.045(±0.08)
R156-D202	5.15 (±2.10)	8.47 (±1.31)	-59.61 (±30.79)	-7.59(±6.46)

**Figure Legends**

**Figure 1.** (a) Superimposed structures of prion protein of four different species: Human, Mouse, Syrian Hamster and Bovine PrP.

(b) Structure of the C-terminal globular domain (residues 125-228) of Wild type human PrP<sup>C</sup> indicating the Y149-D202 hydrogen bond (c) Mutant Y149F, in which residue Y149 in H1 is replaced by a hydrophobic residue phenylalanine.

**Figure 2.** (a) Probability distributions of interaction energy strength between residues Y149-D202 in WT and F149-D202 in Y149F system. (b) Backbone RMS deviations from the starting structure as a function of simulation time (c) Cumulative configurational entropy per C<sub>α</sub> atom of the WT and Y149F systems.

**Figure 3.** Free energy landscape on the plane defined by the first (PC1) and second (PC2) principal components for the a) WT ensemble, and b) the Y149F ensemble. Representative structures for the most populated cluster are depicted.

**Figure 4.** Porcupine plots of the first principal component (PC1) obtained from PCA depicting dominant motions of residues in (a) WT and (b) Y149F of the most populated cluster. The dominant motions in PC1 are illustrated as cones colored in cyan. The length of the arrows represents the amplitude of the cones while the direction indicates the direction of motion. Dynamic Cross-Correlation Map computed for the most populated cluster of c) WT and d) Y149F systems. Axes denote the residue numbers. The color scale for correlation and anti-correlation are shown at the right of each plot.

**Figure 5.** Distance between the sulfur atoms of the disulfide bond Cys179-Cys214 between helices H2-H3 in the most populated cluster for the WT and Y149F systems.

**Figure 6.** The hydrophobic core residues of PrP C-terminal globular domain at (a) H2-H3 interface (b) S1H1 loop-H3 interface. The residues are shown as translucent grey surface, with side chains represented as sticks. (c) Probability distributions of SASA of hydrophobic core residues calculated for cluster 1 obtained from PCA. (d) Per-residue side chain SASA of the hydrophobic core residues.

**Figure 7.** Salt-bridge analyses of the most populated cluster obtained from PCA. Distribution of the H1-H3 inter-domain salt-bridge distance,  $d_{SB}$ , in the most populated cluster obtained from PCA for the residue pairs (a) E146-K204, (b) E146-R208 and (c) E156-D202. Radial distribution functions (RDFs) calculated between the oxygens of the solvent water molecules, and the  $C_{\beta}$  of the salt-bridge forming residues (d) E146 - K204, (e) E146 - R208 and (f) R156 - D202

**Figure 8.** Percentage of secondary structure content per residue in the WT (upper panel) and Y149F (lower panel) systems. The secondary structure assignments were done by STRIDE algorithm in VMD.

## Figures

Figure 1.

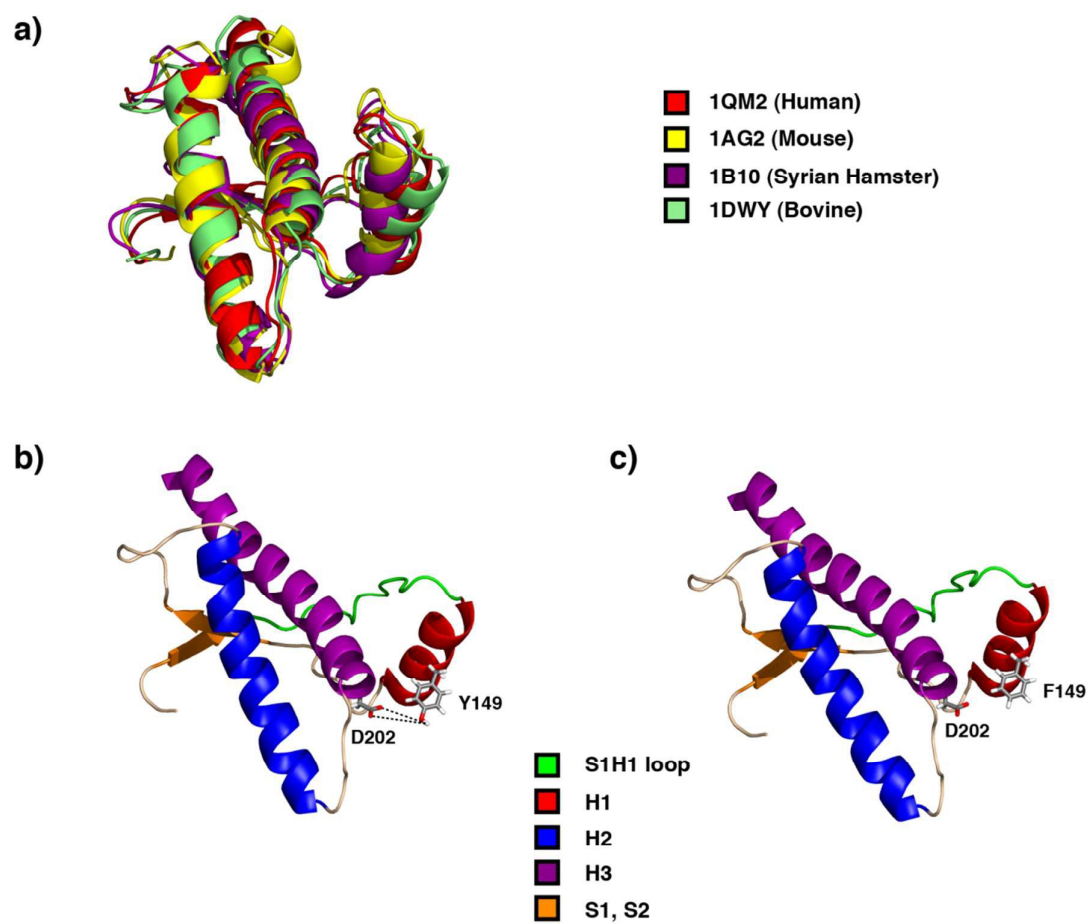


Figure 2.

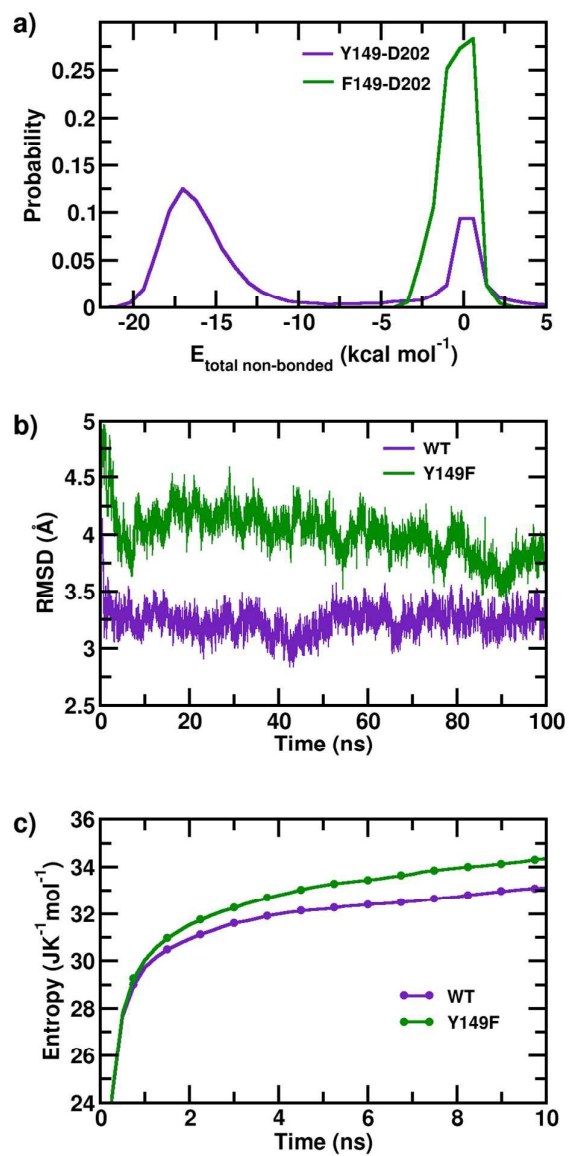


Figure 3.

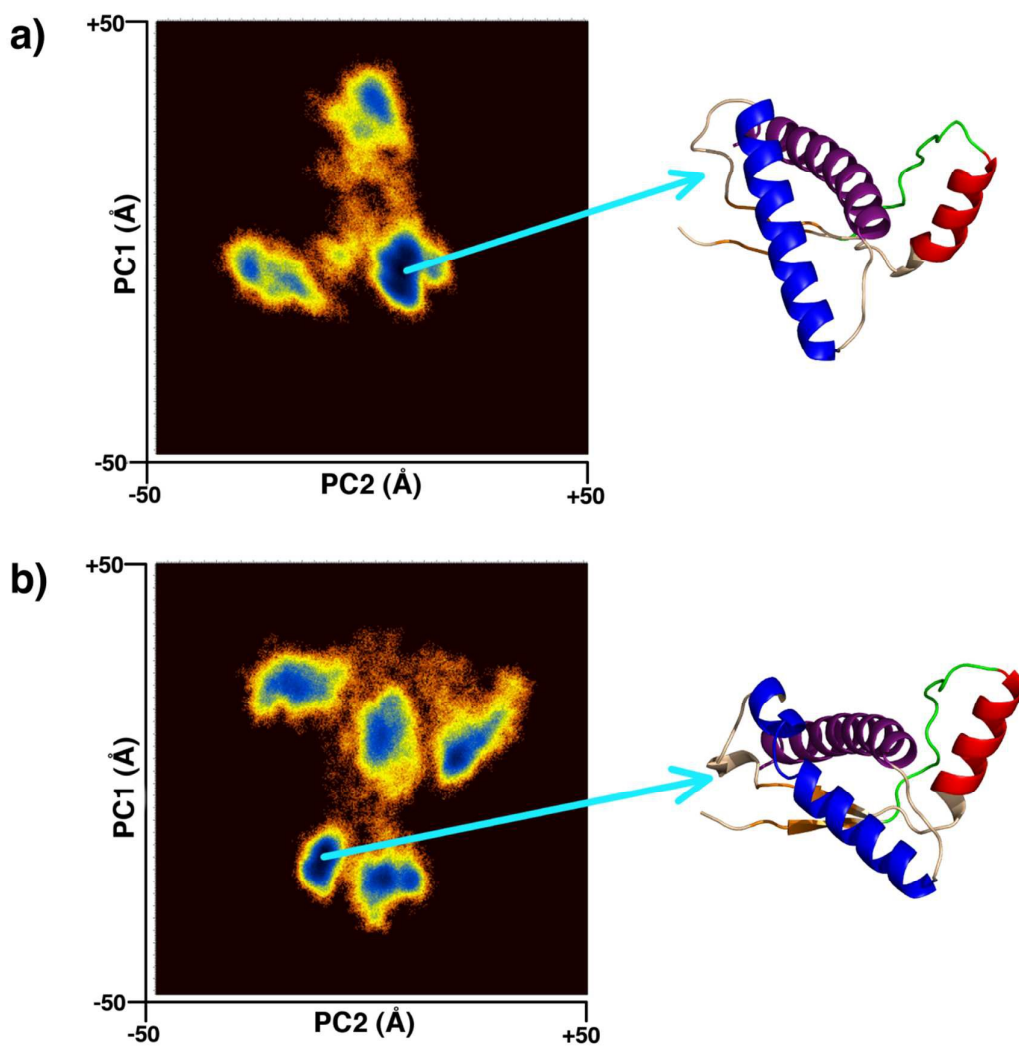
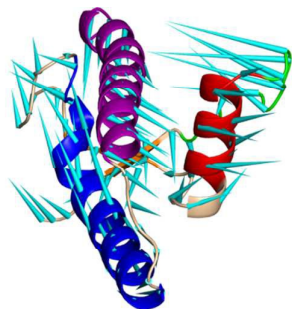


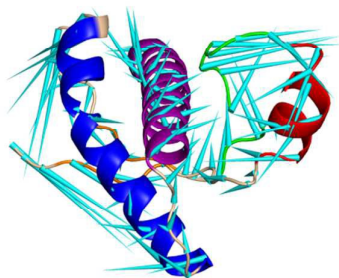
Figure 4.

a)

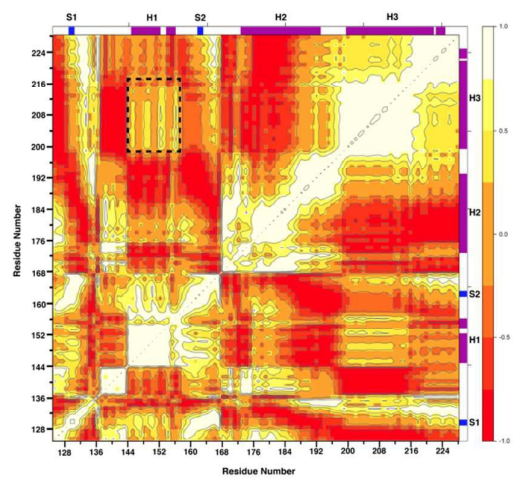


■ S1H1 loop  
■ H1  
■ H2  
■ H3  
■ S1, S2

b)



c)



d)

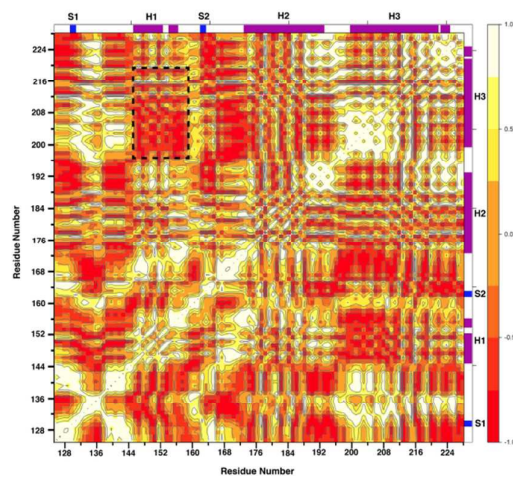


Figure 5.

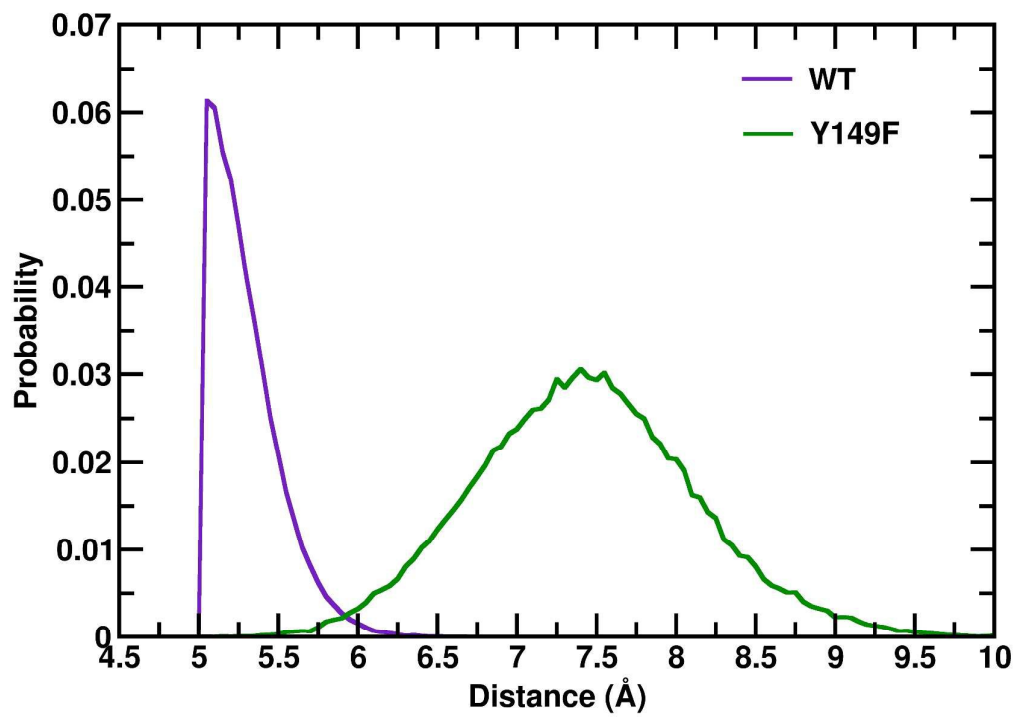


Figure 6.

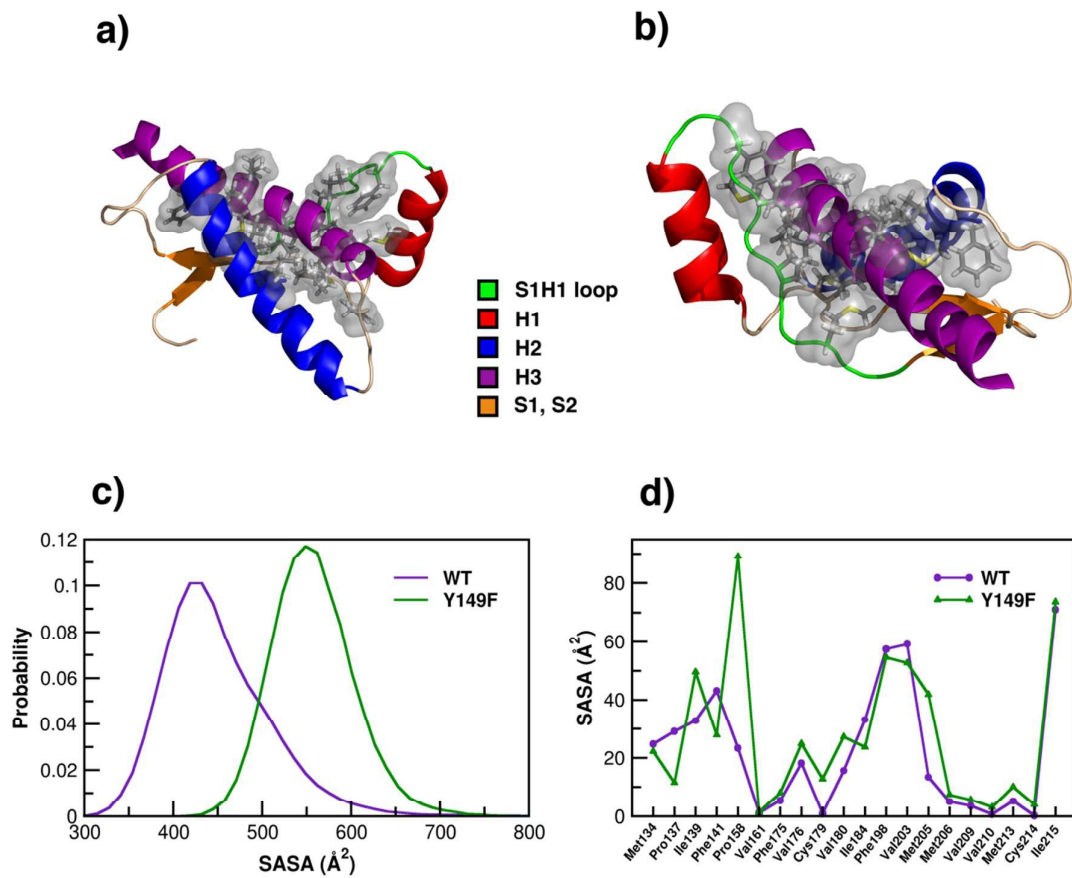


Figure 7.

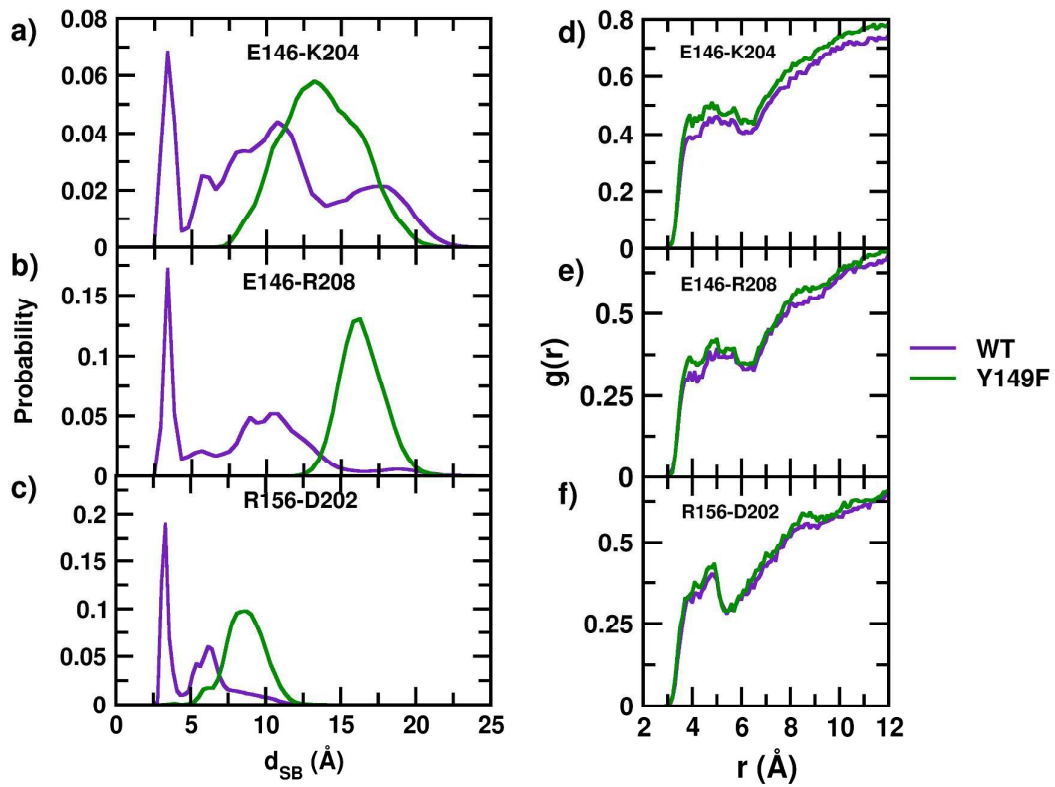


Figure 8.

